Research Square

Preprints are preliminary reports that have not undergone peer review.
They should not be considered conclusive, used to inform clinical practice,
or referenced by the media as validated information.

Outage Performance Analysis of NOMA Assisted UAV-AmBC with Hardware Impairments

Haiyan Huang
Lanzhou Jiaotong University
Yue Bao
Lanzhou Jiaotong University
Yangke Li
Lanzhou Jiaotong University
Huapeng Xu
980637696@qq.com
Lanzhou Jiaotong University
Quanli Xu
China Railway Guangzhou Group Co., Ltd

Research Article

Keywords: Ambient Backscatter Communication (AmBC), Non-Orthogonal Multiple Access (NOMA), Unmanned Aerial Vehicles (UAV), Outage Probability, Ergodic Capacity

Posted Date: July 30th, 2026

DOI: https://doi.org/10.21203/rs.3.rs-10213778/v1

License: This work is licensed under a Creative Commons Attribution 4.0 International License.
Read Full License

Additional Declarations: No competing interests reported.

Outage Performance Analysis of NOMA Assisted UAV-AmBC with Hardware Impairments

Haiyan Huang[1†], Yue Bao[1†], Yangke Li[1†], Huapeng Xu[1*], Quanli Xu[2†]

[1]School of Electronics and Information Engineering, Lanzhou Jiaotong University, Anning West Road, Lanzhou, 730070, China.
[2]Guangzhou Communication Section, China Railway Guangzhou Group Co., Ltd, Huangsha Boulevard, Guangzhou, 510145, China.

*Corresponding author(s). E-mail(s): 980637696@qq.com;
Contributing authors: huanghaiyan@mail.lzjtu.cn; 3041139010@qq.com; 739734029@qq.com; 283806350@qq.com;
†These authors contributed equally to this work.

Abstract

With the rapid increase in the number of Internet of Things (IoT) devices and the growing demand for wireless communication, improving energy efficiency and scaling up network capacity have become a major challenge for next generation wireless communication systems. Ambient backscatter communication (AmBC) and non-orthogonal multiple access (NOMA) are promising techniques for supporting energy-efficient and massive connectivity in future IoT networks, while unmanned aerial vehicles (UAVs) provide flexible coverage when terrestrial links are unavailable or severely blocked. This paper investigates the performance of a NOMA-assisted UAV-AmBC network, where the direct links between the base station and two ground users are blocked. A UAV equipped with a backscatter device acts as a decode-and-forward relay, while the backscatter link provides an additional signal copy to enhance transmission reliability. Considering both perfect and imperfect successive interference cancellation, analytical expressions for the outage probability and ergodic capacity are derived under selection combining (SC) and maximum ratio combining (MRC) schemes. Simulations are provided to validate the theoretical analysis and evaluate the effects of the reflection coefficient, path loss, residual interference, and signal-to-noise ratio. It is shown that imperfect SIC degrades the outage performance, whereas increasing the reflection coefficient improves link reliability. Moreover, MRC achieves lower outage

probability than SC, and the proposed UAV-AmBC-assisted scheme significantly outperforms the benchmark system without AmBC.

Keywords: Ambient Backscatter Communication (AmBC), Non-Orthogonal Multiple Access (NOMA), Unmanned Aerial Vehicles (UAV), Outage Probability, Ergodic Capacity

1 Introduction

The evolution from beyond-5G toward 6G wireless networks is driven by the need to support ubiquitous coverage, massive connectivity, high spectral efficiency, and sustainable low-power operation. These requirements are particularly pressing for the Internet of Things (IoT), where a large number of sensing and monitoring devices are expected to be deployed in smart infrastructure, industrial automation, healthcare, transportation, and environmental monitoring scenarios. Many of these devices are cost-sensitive and energy-constrained, and their batteries may be difficult or even impossible to be replaced after deployment. Therefore, energy-efficient and scalable communication mechanisms have become essential for next-generation IoT networks [1]-[2].

Ambient backscatter communication (AmBC) has emerged as a promising candidate for such low-power networks because it allows passive or semi-passive devices to transmit information by reflecting existing radio-frequency (RF) signals rather than generating dedicated carrier waves. In a typical AmBC system, a backscatter tag harvests energy from incident RF signals and modulates its information by changing the antenna impedance, while the receiver detects the weak reflected signal superimposed on the ambient waveform [3]-[4]. The authors of [5] proposed an AmBC model composed of a single RF source and a passive tag, and investigated the outage performance over real Gaussian channels by deriving exact and asymptotic outage expressions. In contrast to [5], the authors of [6] extended the model to a multi-tag scenario, where multiple tags coexisted and a tag selection mechanism was applied to evaluate system performance. The comparative results showed that the multi-tag configuration achieved improved outage performance over the single-tag counterpart, demonstrating the benefits of spatial diversity and opportunistic tag selection. Additionally, considering the combined effects of hardware impairments and outdated channel state information, the authors of [7] investigated a more practical multi-tag AmBC system and analyzed its performance under imperfect conditions using a low-complexity tag selection scheme. In [8], the authors proposed a mutualistic symbiotic AmBC communication system to address the limitations of conventional passive tag access, enabling spectrum sharing between cellular users and backscatter devices and thereby improving spectral efficiency. From another perspective, [9] introduced an analytical framework to evaluate the covert communication performance of AmBC systems and proposed an optimization scheme to maximize covert throughput under detection constraints. Furthermore, the authors of [10] proposed a relay-assisted mutualistic AmBC communication framework, which achieved a performance tradeoff between

outage probability and resource allocation flexibility under energy availability constraints. These studies established the analytical foundation of AmBC, but most of them focused on terrestrial or infrastructure-fixed systems.

As IoT networks become denser, orthogonal multiple access becomes increasingly inefficient because assigning exclusive time-frequency resources to a large number of devices limits spectral efficiency and connectivity [11]-[12]. Non-orthogonal multiple access (NOMA) addresses this limitation by allowing multiple users to share the same resource block and separating their signals in the power domain through successive interference cancellation (SIC) [13]. The integration of NOMA with backscatter communication has therefore attracted increasing interest [14]. Specifically, the authors of [15] proposed a symbiotic communication network that integrated AmBC with NOMA for IoT devices, achieving spectrum and energy efficiency by enabling IoT transmitters to assist far NOMA users while transmitting their own data. The authors of [16] derived the outage probability and ergodic capacity of an AmBC-NOMA scheme under both perfect and imperfect SIC. Their results showed that the proposed scheme outperformed orthogonal multiple access (OMA) and conventional NOMA in terms of reliability and spectral efficiency. To overcome the limitations of traditional jamming-based covert communication in uplink NOMA systems, the authors of [17] proposed an AmBC system in which the tag simultaneously supported covert signaling and information transmission through a multi-objective optimization approach. Furthermore, the authors of [18] designed a secure AmBC-NOMA system to improve physical-layer security against randomly located eavesdroppers, where artificial noise was introduced and protection zones were established around the transmitter to reduce the risk of interception. These works demonstrated the potential of AmBC-NOMA integration, yet they were still largely constrained by fixed terrestrial deployment and did not fully exploit the spatial flexibility of aerial platforms.

In recent years, unmanned aerial vehicles (UAVs) have attracted significant attention in low-power wireless networks due to their high mobility and flexible deployment capabilities [19]-[20]. These features make UAVs particularly suitable for applications in dynamic or remote areas. In such scenarios, integrating AmBC into mobile UAV platforms provides a practical solution for low-power and large-scale data collection [21]-[22]. For instance, the authors of [23] proposed a UAV-assisted AmBC system and formulated a joint optimization problem to maximize the average transmission rate by jointly designing the UAV trajectory and transmit power. Similarly, the authors of [24] proposed a hybrid BackCom-HTT system supported by drones, where the drones acted as mobile energy sources and assisted multiple IoT nodes operating in backscatter and active transmission modes. To maximize the overall energy efficiency, they optimized key parameters such as the reflection coefficient and time allocation. From another perspective, the authors of [25] investigated the outage performance of a UAV-assisted AmBC system over Nakagami-m fading channels and derived the outage probability and ergodic capacity. In [26], the authors analyzed a UAV-aided network integrating AmBC communication and conventional air-ground transmission, and derived outage probability expressions for both uplink and downlink transmission under mutual interference. To address security issues, the authors of [27] proposed

a UAV-assisted AmBC communication system with cooperative jamming and analyzed the secrecy outage probability under artificial noise interference. Furthermore, the authors of [28] investigated a UAV-aided backscatter communication system with optimized trajectory planning and signal detection, which improved energy efficiency and detection performance for passive devices.

The above studies primarily focused on UAV-assisted AmBC communication systems. However, in scenarios with a large number of users or limited spectrum resources, NOMA can improve spectral efficiency and system capacity by supporting simultaneous transmission over shared resources, thereby providing a scalable solution for connectivity enhancement and resource allocation. Therefore, the authors of [29] proposed a UAV-assisted NOMA backscatter communication system and optimized the sum rate using a block coordinate descent method. In [30], the authors investigated the joint optimization of UAV trajectories in multi-UAV-assisted AmBC communication networks. To maximize the minimum average rate, a solution built on block coordinate descent and successive convex approximation was put forward. Numerical results verified the superiority of the devised method over baseline schemes regarding rate fairness and overall system performance.

From the above studies, it can be seen that the performance optimization and analysis of integrated communication systems combining UAV, AmBC, and NOMA technologies have been widely investigated. It is worth noting that only a few studies have jointly considered UAV, AmBC, and NOMA for analytical performance evaluation. Based on the above analysis, this paper proposes a UAV-assisted AmBC network model with NOMA-based transmission. The communication channels consist of Nakagami-m fading channels over UAV links and Rayleigh fading channels via ambient backscatter devices, and both perfect and imperfect SIC are taken into account. Based on this framework, the end-to-end reliability and capacity performance are analyzed by deriving the outage probability and ergodic capacity under SC and MRC schemes. Specifically, the key contributions of this study are summarized as follows:

i) A NOMA-assisted UAV-AmBC transmission framework is established for scenarios where the direct terrestrial links between the base station and ground users are blocked or severely degraded. In the proposed framework, the UAV serves as an aerial relay, while the backscatter device mounted on the UAV provides an additional reflected signal path. This cooperative transmission strategy enables the ground users to exploit both the UAV forwarding link and the AmBC link, thereby enhancing transmission diversity in obstructed communication environments.

ii) A mixed-channel analytical model is developed to characterize the considered UAV-AmBC network. Specifically, Nakagami-m fading is adopted for the BS-to-UAV and UAV-to-ground-user links, while Rayleigh fading is adopted for the BS-to-backscatter-device and backscatter-device-to-ground-user links. Based on this model, the end-to-end signal-to-interference-plus-noise ratio (SINR) expressions are formulated under both perfect and imperfect SIC, providing the basis for reliability and capacity analysis.

iii) The outage probability and ergodic capacity of the proposed system are derived under two diversity combining schemes, namely SC and MRC. Different from existing

UAV-assisted AmBC or AmBC-NOMA studies that mainly focus on a single transmission path, this work jointly evaluates the UAV relay and backscatter paths to analyze the effect of diversity combining on end-to-end system performance

iv) Through comprehensive simulation experiments, the impact of key system parameters on the proposed network performance was deeply explored, including the backscatter reflection coefficient, path loss, residual interference caused by imperfect SIC, and transmit SNR. In addition, the proposed AmBC-assisted transmission scheme is compared with the benchmark scheme without AmBC, providing design insights into the role of AmBC and diversity combining in improving UAV-assisted NOMA communications.

The remainder of this paper is organized as follows. Section II presents the system model and channel assumptions. Section III derives the analytical outage probability and ergodic capacity under the considered SIC and diversity-combining schemes. Section IV provides numerical and Monte Carlo simulation results. Finally, Section V concludes the paper.

2 SYSTEM MODEL

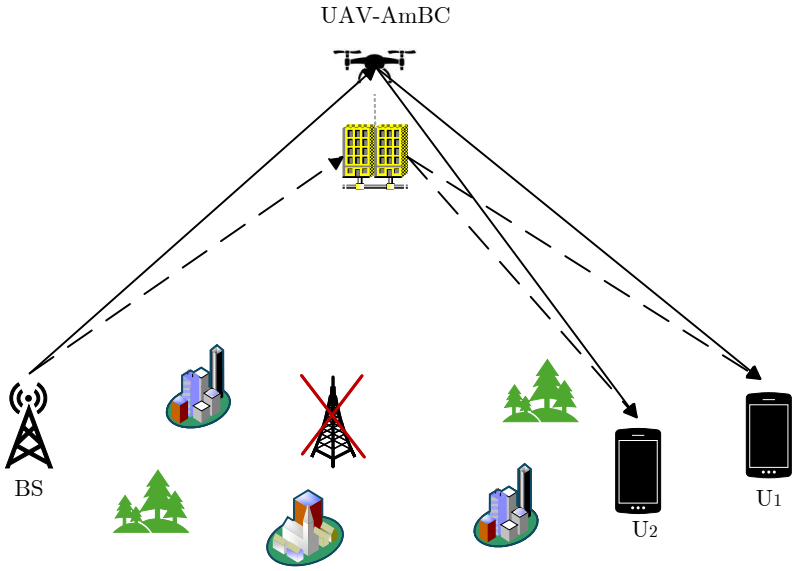


Fig. 1 UAV-AmBC assisted NOMA based network

As shown in Fig. 1, the considered system consists of a Base Station (BS), a Decode-and-Forward (DF) UAV relay equipped with a Backscatter Device (BD), and two ground users, denoted by U_1 and U_2. Due to obstacles or severe shadowing, the direct BS-to-user links are assumed to be unavailable, and all information is delivered through the UAV-assisted transmission. Specifically, the BS first superimposes the information intended for the two users according to the NOMA principle and forwards

the composite signal to the UAV. After decoding, the UAV retransmits the NOMA signal to the ground users through the downlink. Meanwhile, the BD installed on the drone reflects the incident RF signal and reflects information to the user through environmental backscatter communication. Therefore, each user will receive superimposed information from the drone forwarding link and the AmBC link. To improve reception reliability, SC or MRC is employed at the receiver, while both perfect and imperfect SIC are considered during signal detection. The channel coefficients of the BS-to-UAV and UAV-to-user links are denoted by h_{SR} and h_{RU_i}, respectively, whereas those of the BS-to-BD and BD-to-user links are denoted by h_{SB} and h_{BU_i}, where $i \in (1, 2)$. The coordinates of the BS, UAV, and users are given by $(a_0, b_0, 0)$,(x, y, H), $(a_1, b_1, 0)$ and $(a_2, b_2, 0)$. The distances between the links (T-BS-UAV, UAV-U_1 , UAV-U_2) are denoted as d_{sr},d_{ru_1} and d_{ru_2}, where $d_{sr} = \sqrt{(x-a_0)^2 + (y-b_0)^2 + H^2}$,$d_{ru_1} = \sqrt{(x-a_1)^2 + (y-b_1)^2 + H^2}$ and $d_{ru_2} = \sqrt{(x-a_2)^2 + (y-b_2)^2 + H^2}$.

2.1 BS-to-UAV Transmission

In the analysis presented in this paper, two scenarios are assumed: perfect SIC and imperfect SIC. In the perfect SIC scenario, it is assumed that the receiver is able to perfectly decode and subtract the interference from previously received signals. In this ideal case, the SIC process is performed with no errors, allowing each signal to be separated with perfect accuracy, thereby maximizing the system's overall performance. On the other hand, in the imperfect SIC scenario, the receiver faces practical limitations, which prevent the complete elimination of interference. In this case, although SIC is still applied, some residual interference remains in the decoded signals, leading to a degradation in the quality of the received signal and a reduction in overall system performance. In this paper, we take this aspect into account when analyzing the signal transmission and decoding processes. The signal received at the UAV is:

$$y_{UAV}^{i} = \frac{1}{\sqrt{d_{\mathrm{SR}}^{\varsigma}}} h_{\mathrm{SR}} \left(\sum_{i=1}^{2} \sqrt{P_{\mathrm{S}} a_i} x_i \right) + n_i \tag{1}$$

where x_i denote the information transmitted to U_i , here $x_i = \sqrt{P_{\mathrm{S}} a_1} x_1 + \sqrt{P_{\mathrm{S}} a_2} x_2$. P_{S} represents the total transmission power from the BS, and a_i is the power allocation coefficient form BS to UAV. According to the NOMA protocol, we have $\sum_{i=1}^{2} a_i = 1$ and $a_1 > a_2$. h_{SR} denotes the channel fading coefficient, which is assumed to follow a Nakagami-m distribution.ς represents the path-loss exponent and n_i denotes noise at the receiver of U_i . In this model, it is assumed that U_1 is the far user and U_2 is the near user. For U_1 , the received signal at the UAV is:

$$y_{UAV}^{1} = \frac{1}{\sqrt{d_{\mathrm{SR}}^{\varsigma}}} h_{\mathrm{SR}} \left(\sqrt{P_{\mathrm{S}} a_1} x_1 + \sqrt{P_{\mathrm{S}} a_2} x_2 \right) + n_1 \tag{2}$$

After applying perfect SIC, the received signal at the UAV from user U_2 is given by:

$$y_{UAV}^2 = \frac{1}{\sqrt{d_{\mathrm{SR}}^{\varsigma}}} h_{\mathrm{SR}} \sqrt{P_{\mathrm{S}} a_2} x_2 + n_2 \tag{3}$$

When imperfect SIC is applied, the received signal at the UAV from user U_2 is given by:

$$y_{UAV}^1 = \frac{1}{\sqrt{d_{\mathrm{SR}}^{\varsigma}}} h_{\mathrm{SR}} \sqrt{\Upsilon P_{\mathrm{S}} a_1} x_1 + h_{\mathrm{SR}} \sqrt{P_{\mathrm{S}} a_2} x_2 + n_2 \tag{4}$$

where Υ denotes the error factor associated with imperfect SIC; when $\Upsilon = 0$, it corresponds to the case of perfect SIC.

In the first hop of the transmission process, the received signal at the UAV is given by (1). The signal-to-interference-plus-noise ratio (SINR) for decoding the information of user U_1 at the UAV can be expressed as follows:

$$\gamma_1 = \frac{a_1 \rho |h_{\mathrm{SR}}|^2}{a_2 \rho |h_{\mathrm{SR}}|^2 + d_{\mathrm{SR}}^{\varsigma}} \tag{5}$$

where$\rho = \frac{P_{\mathrm{S}}}{\sigma_1^2}$, and σ_1^2 is the noise power of U_1.

When perfect SIC is employed, the signal-to-noise ratio (SNR) for decoding the information of U_2 is given by:

$$\gamma_2^{\mathrm{per}} = \frac{a_2 \rho |h_{\mathrm{SR}}|^2}{d_{\mathrm{SR}}^{\varsigma}} \tag{6}$$

where$\rho = \frac{P_{\mathrm{S}}}{\sigma_2^2}$, and σ_2^2 is the noise power of U_2. Assuming $\sigma_1^2 = \sigma_2^2$.

When imperfect SIC is employed, the SNR for decoding the information of U_2 is given by:

$$\gamma_2^{\mathrm{imp}} = \frac{a_2 \rho |h_{\mathrm{SR}}|^2}{\Upsilon a_1 \rho |h_{\mathrm{SR}}|^2 + d_{\mathrm{SR}}^{\varsigma}} \tag{7}$$

2.2 UAV Energy Harvesting and Relay Forwarding

By utilizing time-switching relay schemes, the UAV relay obtains energy from the RF signals transmitted by the BS. Hence, the energy level acquired at the UAV relay is:

$$E_{UAV} = \frac{\alpha \beta P_{\mathrm{S}} |h_{\mathrm{SR}}|^2}{d_{\mathrm{SR}}^{\varsigma}} T \tag{8}$$

where α represents the fraction of the EH time, T is the total time period and β denotes the EH efficiency.

The transmit power of the relay is determined by the amount of energy harvested during the first phase. It is expressed as follows:

$$P_{\mathrm{U}} = \frac{E_{UAV}}{(1-\alpha)\frac{T}{2}} = \frac{2\alpha\beta P_{\mathrm{S}} |h_{\mathrm{SR}}|^2}{(1-\alpha) d_{\mathrm{SR}}^{\varsigma}} \tag{9}$$

The UAV relay forwards the information to the ground users using the harvested energy. During the second phase of transmission, the signal received at U_i from the UAV is:

$$y_{\mathrm{U}}^{i}=\frac{1}{\sqrt{d_{\mathrm{RU}_i}^{\varsigma}}}h_{\mathrm{RU}_i}\left(\sqrt{P_{\mathrm{U}}a_{\mathrm{U},1}}x_1+\sqrt{P_{\mathrm{U}}a_{\mathrm{U},2}}x_2\right)+n_{\mathrm{U}_i} \tag{10}$$

where h_{RU_i} denotes the channel fading coefficient of the UAV-to-U_i link, which is assumed to follow a Nakagami-m distribution. $a_{\mathrm{U},i}$ denotes the power allocation factor for i^{th} user, and $\sum_{i=1}^{2}a_{\mathrm{U},i}=1$. n_{U_i} represents the noise at the i^{th} ground user.

At U_2 , the SINR for decoding the information of U_1 is:

$$\gamma_{\mathrm{U2},1}=\frac{\mathrm{H}a_{\mathrm{U},1}|h_{\mathrm{SR}}|^2|h_{\mathrm{RU}_2}|^2}{\mathrm{H}a_{\mathrm{U},2}|h_{\mathrm{SR}}|^2|h_{\mathrm{RU}_2}|^2+d_{\mathrm{SR}}^{\varsigma}d_{\mathrm{RU}_2}^{\varsigma}} \tag{11}$$

where $\mathrm{H}=\frac{2\alpha\beta}{1-\beta}$.

When perfect SIC is employed, the SINR for decoding the information of U_2 is given by:

$$\gamma_{\mathrm{U2},2}=\frac{\mathrm{H}a_{\mathrm{U},2}\rho|h_{\mathrm{SR}}|^2|h_{\mathrm{RU}_2}|^2}{d_{\mathrm{SR}}^{\varsigma}d_{\mathrm{RU}_2}^{\varsigma}} \tag{12}$$

When imperfect SIC is employed, the SINR for decoding the information of U_2 is given by:

$$\gamma_{\mathrm{U2},2}^{\mathrm{imp}}=\frac{\mathrm{H}a_{\mathrm{U},2}\rho|h_{\mathrm{SR}}|^2|h_{\mathrm{RU}_2}|^2}{\Upsilon\mathrm{H}a_{\mathrm{U},1}\rho|h_{\mathrm{SR}}|^2|h_{\mathrm{RU}_2}|^2+d_{\mathrm{SR}}^{\varsigma}d_{\mathrm{RU}_2}^{\varsigma}} \tag{13}$$

At U_1 , the received SINR can be expressed as:

$$\gamma_{\mathrm{U1},1}=\frac{\mathrm{H}a_{\mathrm{U},1}\rho|h_{\mathrm{SR}}|^2|h_{\mathrm{RU}_1}|^2}{\mathrm{H}a_{\mathrm{U},2}\rho|h_{\mathrm{SR}}|^2|h_{\mathrm{RU}_1}|^2+d_{\mathrm{SR}}^{\varsigma}d_{\mathrm{RU}_1}^{\varsigma}} \tag{14}$$

2.3 AmBC-assisted Transmission

Based on the system model, the received signals at ground users U_i can be expressed as

$$y_{\mathrm{BC}}^{\mathrm{U}_i}=\eta h_{\mathrm{SB}}h_{\mathrm{BU}_i}x_{\mathrm{B}}\left(\sqrt{P_{\mathrm{S}}a_1}x_1+\sqrt{P_{\mathrm{S}}a_2}x_2\right)+n_2 \tag{15}$$

where η represents the backscatter coefficient. h_{SB} denotes the channel fading coefficient between the BS and the BD, which is assumed to follow a Rayleigh distribution; h_{BU_i} denotes the channel fading coefficient between the BD and the ground users U_i , which is assumed to follow a Rayleigh distribution. x_B represents the signal from the backscatter device itself. n_2 represents the additive Gaussian white noise at U_i in the backscattering link.

The SNR at U_1 can be expressed as:

$$\gamma_{\mathrm{U1}}^{\mathrm{BC}}=\frac{\eta^2a_1P_{\mathrm{S}}|h_{\mathrm{SB}}|^2|h_{\mathrm{BU}_1}|^2}{\eta^2a_2P_{\mathrm{S}}|h_{\mathrm{SB}}|^2|h_{\mathrm{BU}_1}|^2+{\sigma_1}^2} \tag{16}$$

When perfect SIC is employed, the SNR for decoding the information of U_2 is given by:

$$\gamma_{\mathrm{U2}}^{\mathrm{BC}} = \frac{\eta^2 a_2 P_{\mathrm{S}} |h_{\mathrm{SB}}|^2 |h_{\mathrm{BU}_2}|^2}{\sigma_2^2} \tag{17}$$

When imperfect SIC is employed, the SNR for decoding the information of U_2 is given by:

$$\gamma_{\mathrm{U2}}^{\mathrm{imp,BC}} = \frac{\eta^2 a_2 P_{\mathrm{S}} |h_{\mathrm{SB}}|^2 |h_{\mathrm{BU}_2}|^2}{\Upsilon \eta^2 a_1 P_{\mathrm{S}} |h_{\mathrm{SB}}|^2 |h_{\mathrm{BU}_2}|^2 + {\sigma_2}^2} \tag{18}$$

2.4 SC and MRC Combining

The effective SINR of users undergoing two-hop communication via the UAV is given as:

$$M = \min\left(\gamma_i, \gamma_{\mathrm{U}_i,i}\right) \tag{19}$$

where γ_i denotes the SINR of user U_i at the UAV. $\gamma_{U_i,i}$ denotes the SINR at user U_i after transmission through the UAV.

The expressions for these two SNRs have been discussed in detail in Section 2. Therefore, the Cumulative Distribution Function (CDF) of the SINR for users served via the UAV is given as follows:

$$\begin{aligned} F_M\left(\gamma_{th}\right) &= P\left(M \leq \gamma_{th}\right) \\ &= P\left(\min\left(\gamma_i, \gamma_{\mathrm{U}_i,i}\right) \leq \gamma_{th}\right) \\ &= 1 - P\left(\min\left(\gamma_i, \gamma_{\mathrm{U}_i,i}\right) > \gamma_{th}\right) \\ &= 1 - P\left(\gamma_i > \gamma_{th}\right) P\left(\gamma_{\mathrm{U}_i,i} > \gamma_{th}\right) \\ &= 1 - \left[1 - F_{\gamma_i}\left(\gamma_{th}\right)\right]\left[1 - F_{\gamma_{\mathrm{U}_i,i}}\left(\gamma_{th}\right)\right] \end{aligned} \tag{20}$$

The ground user receives signals transmitted from both the UAV and the AmBC link. Under the SC strategy, the user selects the better link. Accordingly, the SINR under the SC scheme can be expressed as:

$$N = \max\left(M, \gamma_{\mathrm{U}_i}^{\mathrm{BC}}\right) \tag{21}$$

where $\gamma_{\mathrm{U}_i}^{\mathrm{BC}}$ denotes the end-to-end SINR at user resulting from the AmBC transmission. When employing the MRC technique, the overall SINR at user U_i is calculated as the sum of two components $Z_{mr} = X_{mr} + Y_{mr}$, where X_{mr} is defined as M , and Y_{mr} corresponds to $\gamma_{\mathrm{U}_i}^{\mathrm{BC}}$.

3 OUTAGE AND ERGODIC CAPACITY PERFORMANCE ANALYSIS

The effective SNR/SINR of the communication links from the BS to UAV-BC and from UAV-BC to ground users has been described in Section 2. Based on the perfect and imperfect SIC scenarios at the UAV and ground users considered in that section, the outage probability and achievable ergodic capacity at the receiver side are analyzed.

3.1 User Outage Probability for SC Scheme

Outage probability quantifies the likelihood that the received SINR fails to meet a required quality-of-service threshold γ_{th} , thus indicating a disruption in reliable transmission. Under the SC strategy, the optimal communication link from the source to the destination can be selected based on signals received through the UAV or AmBC, aiming to maximize the SINR for ground users while ensuring it remains below the threshold γ_{th} .When the SC scheme is applied, the outage probability of the end-to-end link at U_1 can be expressed as:

$$\begin{aligned} P_{\mathrm{OUT}}^{\mathrm{SC,U_1}} &= P\left(\max\left(M, \gamma_{\mathrm{U_1}}^{\mathrm{BC}}\right) \leq \gamma_{th}\right) \\ &= P\left(\gamma_{\mathrm{U_1}}^{\mathrm{BC}} \leq \gamma_{th},\ \min\left(\gamma_1, \gamma_{\mathrm{U}_1,1}\right) \leq \gamma_{th}\right) \\ &= P\left(\gamma_{\mathrm{U_1}}^{\mathrm{BC}} \leq \gamma_{th}\right) \cdot P\left(\min\left(\gamma_1, \gamma_{\mathrm{U}_1,1}\right) \leq \gamma_{th}\right) \\ &= F_{\gamma_{\mathrm{U_1}}^{\mathrm{BC}}}\left(\gamma_{th}\right) \cdot \left[F_{\gamma_1}\left(\gamma_{th}\right) + F_{\gamma_{\mathrm{U}_1,1}}\left(\gamma_{th}\right) - F_{\gamma_1}\left(\gamma_{th}\right) F_{\gamma_{\mathrm{U}_1,1}}\left(\gamma_{th}\right)\right] \end{aligned} \tag{22}$$

The PDF and CDF of a single Nakagami-m faded channel can be described by the following expressions:

$$f_{\gamma_1}(x) = \frac{2{m_i}^{m_i}}{\Gamma(m_i)\,\bar{\Omega}_i^{m_i}} x^{2m_i-1} \exp\left(-\frac{m_i x^2}{\bar{\Omega}_i}\right) \tag{23}$$

where m_i is the fading shape parameter, $\bar{\Omega}_i$ denotes the average power of the fading envelope, typically defined as $\mathrm{E}[x^2]$, representing the mean received signal power. $\Gamma(\cdot)$ is the Gamma function.

The CDF of γ_1 and γ_2 under a single Nakagami-m fading channel can be written as:

$$F_{\gamma_1}\left(\gamma_{th}\right) = \gamma\left(m_1, \frac{m_1}{\bar{\Omega}_1}\left(\frac{\gamma_{th}}{B_1 - B_2\gamma_{th}}\right)^2\right) \tag{24}$$

where γ denotes the incomplete gamma function. Under the assumption of perfect SIC, the corresponding CDF of γ_2 is given by:

$$F_{\gamma_2}\left(\gamma_{th}\right) = \gamma\left(m_2, \frac{m_2}{\bar{\Omega}_2}\left(\frac{\gamma_{th}}{B_2}\right)^2\right) \tag{25}$$

where $B_1 = \frac{a_1\rho}{d_{\mathrm{SR}}^{\varsigma}}$, and $B_2 = \frac{a_2\rho}{d_{\mathrm{SR}}^{\varsigma}}$. Under the assumption of imperfect SIC, the corresponding CDF of γ_2^{imp} is given by:

$$F_{\gamma_2^{\mathrm{imp}}}\left(\gamma_{th}\right) = \gamma\left(m_2, \frac{m_2}{\bar{\Omega}_2}\left(\frac{\gamma_{th}}{B_2 - B_3\gamma_{th}}\right)^2\right) \tag{26}$$

where $B_3 = \frac{\Upsilon a_1 \rho}{d_{\mathrm{SR}}^{\varsigma}}$. The CDF of $\gamma_{\mathrm{U}_1,1}$ and $\gamma_{\mathrm{U}_2,2}$ can be written as:

$$
\begin{aligned}
&F_{\gamma_{\mathrm{U}_1,1}}(\gamma_{th}) \\
&= P(\gamma_{\mathrm{U}_1,1} \leq \gamma_{th}) \\
&= P\left(\frac{\mathrm{H}a_{\mathrm{U},1}\rho |h_{\mathrm{SR}}|^2 |h_{\mathrm{RU}_1}|^2}{\mathrm{H}a_{\mathrm{U},2}\rho |h_{\mathrm{SR}}|^2 |h_{\mathrm{RU}_1}|^2 + d_{\mathrm{SR}}^{\varsigma} d_{\mathrm{RU}_1}^{\varsigma}} \leq \gamma_{th}\right) \\
&= P\left(|h_{\mathrm{SR}}|^2 |h_{\mathrm{RU}_1}|^2 \leq \frac{\gamma_{th}}{B_4 - B_5\gamma_{th}}\right) \\
&= P\left(\int_0^{\frac{\gamma_{th}}{B_4 - B_5\gamma_{th}}} \frac{4x^{m_1+m_2-1} m_1^{m_1} m_2^{m_2}}{\Gamma(m_1)\Gamma(m_2)(\Omega_1\Omega_2)^{\frac{m_1+m_2}{2}}} K_{m_1-m_2}\left(2x\sqrt{\frac{m_1 m_2}{\Omega_1\Omega_2}}\right) dx\right) \qquad (27) \\
&= \left(\frac{m_1}{m_2}\right)^{\frac{m_1-m_2}{2}} \frac{\left(\frac{\gamma_{th}}{B_4 - B_5\gamma_{th}}\right)^{m_1+m_2}}{\Gamma(m_2)\Gamma(m_1+1)} \\
&\quad \times G_{1,3}^{3,1}\left(-\frac{m_1 m_2}{\Omega_1\Omega_2}\left(\frac{\gamma_{th}}{B_4 - B_5\gamma_{th}}\right)^2 \middle| \begin{matrix} 1 - \frac{m_1+m_2}{2} \\ 1 - m_2, \quad -m_1, \quad 0 \end{matrix}\right)
\end{aligned}
$$

where$B_4 = \frac{\mathrm{H}a_{\mathrm{U},1}\rho}{d_{\mathrm{SR}}^{\varsigma} d_{\mathrm{RU}_1}^{\varsigma}}$, and $B_5 = \frac{\mathrm{H}a_{\mathrm{U},2}\rho}{d_{\mathrm{SR}}^{\varsigma} d_{\mathrm{RU}_2}^{\varsigma}}$.

See Appendix A.

Under the assumption of perfect SIC, Similarly, the CDF of $\gamma_{\mathrm{U}_2,2}$ can be expressed as:

$$
\begin{aligned}
&F_{\gamma_{\mathrm{U}_2,2}}(\gamma_{th}) \\
&= P(\gamma_{\mathrm{U}_2,2} \leq \gamma_{th}) \\
&= P\left(\frac{\mathrm{H}a_{\mathrm{U},2}\rho |h_{\mathrm{SR}}|^2 |h_{\mathrm{RU}_2}|^2}{d_{\mathrm{SR}}^{\varsigma} d_{\mathrm{RU}_2}^{\varsigma}} \leq \gamma_{th}\right) \\
&= P\left(|h_{\mathrm{SR}}|^2 |h_{\mathrm{RU}_2}|^2 \leq \frac{\gamma_{th}}{B_6}\right) \\
&= P\left(\int_0^{\frac{\gamma_{th}}{B_6}} \frac{4x^{m_1+m_2-1} m_1^{m_1} m_2^{m_2}}{\Gamma(m_1)\Gamma(m_2)(\Omega_1\Omega_2)^{\frac{m_1+m_2}{2}}} K_{m_1-m_2}\left(2x\sqrt{\frac{m_1 m_2}{\Omega_1\Omega_2}}\right) dx\right) \qquad (28) \\
&= \left(\frac{m_1}{m_2}\right)^{\frac{m_1-m_2}{2}} \frac{\left(\frac{\gamma_{th}}{B_6}\right)^{m_1+m_2}}{\Gamma(m_2)\Gamma(m_1+1)} \\
&\quad \times G_{1,3}^{3,1}\left(-\frac{m_1 m_2}{\Omega_1\Omega_2}\left(\frac{\gamma_{th}}{B_6}\right)^2 \middle| \begin{matrix} 1 - \frac{m_1+m_2}{2} \\ 1 - m_2, \quad -m_1, \quad 0 \end{matrix}\right)
\end{aligned}
$$

For the case of imperfect SIC, the CDF of $\gamma_{\mathrm{U}_2,2}^{\mathrm{imp}}$ remains identical to that in equation (27), except that B_4 and B_5 are replaced by B_6 and B_7, respectively, where $B_6 = \frac{\mathrm{H}a_{\mathrm{U},2}\rho}{d_{\mathrm{SR}}^{\varsigma} d_{\mathrm{RU}_2}^{\varsigma}}$ and $B_7 = \frac{\Upsilon \mathrm{H}a_{\mathrm{U},1}\rho}{d_{\mathrm{SR}}^{\varsigma} d_{\mathrm{RU}_2}^{\varsigma}}$.

The PDF and CDF of a single Rayleigh faded channel can be described by the following expressions:

$$f_{\gamma_{U_i,i}}(x) = \frac{1}{\lambda_i} \exp\left(-\frac{1}{\lambda_i} x\right) \qquad (29)$$

$$F_{\gamma_{U_i,i}}(x) = 1 - \exp\left(-\frac{1}{\lambda_i}x\right) \tag{30}$$

where λ_i denotes the scale parameter of the Rayleigh distribution.

The CDF of $\gamma_{U_1}^{BC}$ product of two independent Rayleigh fading variables can be written as:

$$\begin{aligned}
&F_{\gamma_{U_1}^{BC}}(\gamma_{th}) \\
&= P\left(\gamma_{U_1}^{BC} \le \gamma_{th}\right) \\
&= P\left(\frac{\eta^2 a_1 P_S |h_{SB}|^2 |h_{BU_1}|^2}{\eta^2 a_2 P_S |h_{SB}|^2 |h_{BU_1}|^2 + \sigma_1^2} \le \gamma_{th}\right) \\
&= P\left(|h_{SB}|^2 |h_{BU_1}|^2 \le \frac{\gamma_{th}\sigma_1^2}{\eta^2 a_1 P_S - \eta^2 a_2 P_S \gamma_{th}}\right) \\
&= \int_0^\infty \int_0^{\frac{\gamma_{th}\sigma_1^2}{(\eta^2 a_1 P_S - \eta^2 a_2 P_S \gamma_{th})y}} f_X(x) f_Y(y)\, dxdy \\
&= 1 - \frac{1}{\lambda_2}\sqrt{\frac{\gamma_{th}\sigma_1^2\lambda_2}{\lambda_1(\eta^2 a_1 P_S - \eta^2 a_2 P_S \gamma_{th})}}\left[K_1\left(2\sqrt{\frac{\gamma_{th}\sigma_1^2}{\lambda_1\lambda_2(\eta^2 a_1 P_S - \eta^2 a_2 P_S \gamma_{th})}}\right)\right]
\end{aligned} \tag{31}$$

See Appendix B.

Similar to equation (31), the CDF of $\gamma_{U_2}^{BC}$ can be obtained as:

$$\begin{aligned}
F_{\gamma_{U_2}^{BC}}(\gamma_{th}) &= P\left(\gamma_{U2}^{BC} \le \gamma_{th}\right) \\
&= P\left(\frac{\eta^2 a_2 P_S |h_{SB}|^2 |h_{BU_2}|^2}{\sigma_2^2} \le \gamma_{th}\right) \\
&= P\left(|h_{SB}|^2 |h_{BU_2}|^2 \le \frac{\gamma_{th}\sigma_2^2}{\eta^2 a_2 P_S}\right) \\
&= \int_0^\infty \int_0^{\frac{\gamma_{th}\sigma_2^2}{\eta^2 a_2 P_S y}} f_X(x) f_Y(y)\, dxdy \\
&= 1 - \frac{1}{\lambda_2}\sqrt{\frac{\gamma_{th}\sigma_2^2\lambda_2}{\lambda_1\eta^2 a_2 P_S}} K_1\left(2\sqrt{\frac{\gamma_{th}\sigma_2^2}{\lambda_1\lambda_2\eta^2 a_2 P_S}}\right)
\end{aligned} \tag{32}$$

Under the assumption of imperfect SIC, the corresponding CDF of $\gamma_{U_2}^{imp,BC}$ is given by:

$$\begin{aligned}
&F_{\gamma_{U_2}^{imp,BC}}(\gamma_{th}) \\
&= P\left(\gamma_{U_2}^{imp,BC} \le \gamma_{th}\right) \\
&= P\left(\frac{\eta^2 a_2 P_S |h_{SB}|^2 \left|h_{BU_2}\right|^2}{\Upsilon\eta^2 a_1 P_S |h_{SB}|^2 \left|h_{BU_2}\right|^2 + {\sigma_2}^2} \le \gamma_{th}\right) \\
&= P\left(|h_{SB}|^2 |h_{BU_2}|^2 \le \frac{\gamma_{th}\sigma_2^2}{(\eta^2 a_2 P_S - \Upsilon\eta^2 a_1 P_S \gamma_{th})}\right) \\
&= 1 - \frac{1}{\lambda_2}\sqrt{\frac{\gamma_{th}\sigma_2^2\lambda_2}{\lambda_1(\eta^2 a_2 P_S - \Upsilon\eta^2 a_1 P_S \gamma_{th})}} K_1\left(2\sqrt{\frac{\gamma_{th}\sigma_2^2}{\lambda_1\lambda_2(\eta^2 a_2 P_S - \Upsilon\eta^2 a_1 P_S \gamma_{th})}}\right)
\end{aligned} \tag{33}$$

At present, the Outage probabilities under different conditions are discussed:

1) Under the assumption of perfect SIC, the outage probability at U_1 is given by:

$$
\begin{aligned}
&P_{\mathrm{OUT}}^{\mathrm{SC,U_1}} \\
&= 1 - \frac{1}{\lambda_2}\sqrt{\frac{\gamma_{th}\sigma_1^2\lambda_2}{\lambda_1\left(\eta^2 a_1 P_{\mathrm{S}} - \eta^2 a_2 P_{\mathrm{S}}\gamma_{th}\right)}}K_1\left(2\sqrt{\frac{\gamma_{th}\sigma_1^2}{\lambda_1\lambda_2\left(\eta^2 a_1 P_{\mathrm{S}} - \eta^2 a_2 P_{\mathrm{S}}\gamma_{th}\right)}}\right) \\
&\quad\times\left\{\begin{array}{l}
\left(\frac{m_1}{m_2}\right)^{\frac{m_1-m_2}{2}}\frac{\left(\frac{\gamma_{th}}{B_4-B_5\gamma_{th}}\right)^{m_1+m_2}}{\Gamma(m_2)\Gamma(m_1+1)} \\
\times G_{1,3}^{3,1}\left(-\frac{m_1 m_2}{\Omega_1\Omega_2}\left(\frac{\gamma_{th}}{B_4-B_5\gamma_{th}}\right)^2\middle|\begin{array}{ccc} 1-\frac{m_1+m_2}{2} & \\ 1-m_2, & -m_1, \quad 0\end{array}\right) \\
\times\left[\gamma\left(m_1, \frac{m_1}{\bar{\Omega}_1}\left(\frac{\gamma_{th}}{B_1-B_2\gamma_{th}}\right)^2\right)+1\right]+\gamma\left(m_1, \frac{m_1}{\bar{\Omega}_1}\left(\frac{\gamma_{th}}{B_1-B_2\gamma_{th}}\right)^2\right)
\end{array}\right\}
\end{aligned}
\tag{34}
$$

2) Under the assumption of perfect SIC, the outage probability at U_2 is given by:

$$
\begin{aligned}
P_{\mathrm{OUT}}^{\mathrm{SC,U_2}} &= 1 - \frac{1}{\lambda_2}\sqrt{\frac{\gamma_{th}\sigma_2^2\lambda_2}{\lambda_1\eta^2 a_2 P_{\mathrm{S}}}}K_1\left(2\sqrt{\frac{\gamma_{th}\sigma_2^2}{\lambda_1\lambda_2\eta^2 a_2 P_{\mathrm{S}}}}\right) \\
&\quad\times\left\{\begin{array}{l}
\left(\frac{m_1}{m_2}\right)^{\frac{m_1-m_2}{2}}\frac{\left(\frac{\gamma_{th}}{B_6}\right)^{m_1+m_2}}{\Gamma(m_2)\Gamma(m_1+1)} \\
\times G_{1,3}^{3,1}\left(-\frac{m_1 m_2}{\Omega_1\Omega_2}\left(\frac{\gamma_{th}}{B_6}\right)^2\middle|\begin{array}{ccc} 1-\frac{m_1+m_2}{2} & \\ 1-m_2, & -m_1, \quad 0\end{array}\right) \\
\times\left[\gamma\left(m_2, \frac{m_2}{\bar{\Omega}_2}\left(\frac{\gamma_{th}}{B_2}\right)^2\right)+1\right]+\gamma\left(m_2, \frac{m_2}{\bar{\Omega}_2}\left(\frac{\gamma_{th}}{B_2}\right)^2\right)
\end{array}\right\}
\end{aligned}
\tag{35}
$$

3) Under the assumption of imperfect SIC, the outage probability at U_1 is given by:

When imperfect SIC is employed, the outage probability at U_1 is identical to that under perfect SIC.

$$
P_{\mathrm{OUT}}^{\mathrm{SC,imp,U_1}} = P_{\mathrm{OUT}}^{\mathrm{SC,U_1}} \tag{36}
$$

4) Under the assumption of imperfect SIC, the outage probability at U_2 is given by:

$$
\begin{aligned}
&P_{\mathrm{OUT}}^{\mathrm{SC,imp,U_2}} \\
&= 1 - \frac{1}{\lambda_2}\sqrt{\frac{\gamma_{th}\sigma_2^2\lambda_2}{\lambda_1\left(\eta^2 a_2 P_{\mathrm{S}} - \Upsilon\eta^2 a_1 P_{\mathrm{S}}\gamma_{th}\right)}}K_1\left(2\sqrt{\frac{\gamma_{th}\sigma_2^2}{\lambda_1\lambda_2\left(\eta^2 a_2 P_{\mathrm{S}} - \Upsilon\eta^2 a_1 P_{\mathrm{S}}\gamma_{th}\right)}}\right) \\
&\times\left\{\begin{array}{l}
\left(\frac{m_1}{m_2}\right)^{\frac{m_1-m_2}{2}}\frac{\left(\frac{\gamma_{th}}{B_6 - B_7\gamma_{th}}\right)^{m_1+m_2}}{\Gamma(m_2)\Gamma(m_1+1)} \\
\times G_{1,3}^{3,1}\left(-\frac{m_1 m_2}{\Omega_1\Omega_2}\left(\frac{\gamma_{th}}{B_6 - B_7\gamma_{th}}\right)^2\middle|\begin{array}{ccc} 1-\frac{m_1+m_2}{2} & \\ 1-m_2, & -m_1, \quad 0\end{array}\right) \\
\times\left[\gamma\left(m_2, \frac{m_2}{\bar{\Omega}_2}\left(\frac{\gamma_{th}}{B_2 - B_3\gamma_{th}}\right)^2\right)+1\right] + \gamma\left(m_2, \frac{m_2}{\bar{\Omega}_2}\left(\frac{\gamma_{th}}{B_2 - B_3\gamma_{th}}\right)^2\right)
\end{array}\right\}
\end{aligned}
\tag{37}
$$

3.2 User Outage Probability for MRC Scheme

MRC improves signal reception by coherently combining multiple received signals to maximize the SNR. Since outage probability depends on whether the received SNR falls below a predefined threshold, MRC has a direct impact on it. Therefore, in the following analysis, we employ MRC to evaluate the outage probability under the considered system model. The outage probability expression at U_i is given by:

$$
\begin{aligned}
P_{\mathrm{OUT}}^{\mathrm{MRC,U_i}} &= P\left((X+Y) \le \gamma_{th}\right) \\
&= \int_{y=0}^{\gamma_{th}} F_{X_{mr}}(\gamma_{th}-y) f_{Y_{mr}}(y) dy
\end{aligned}
\tag{38}
$$

1) Under the assumption of perfect SIC, the outage probability at U_1 is given by:

$$
\begin{aligned}
P_{\mathrm{OUT}}^{\mathrm{MRC,U_1}} &= \int_{y=0}^{\gamma_{th}}\left[1-\left(1-F_{\gamma_1}(\gamma_{th}-y)\right)\left(1-F_{\gamma_{U_1,1}}(\gamma_{th}-y)\right) f_{\gamma_{U_1}^{BC}}(y)\right] dy \\
&= \int_{y=0}^{\gamma_{th}}\left[\begin{array}{l}
1-\left(1-F_{\gamma_1}(\gamma_{th}-y)\right)\left(1-F_{\gamma_{U_1,1}}(\gamma_{th}-y)\right) \\
\times\frac{1}{\lambda_2}\left[\frac{-\eta^2 a_2 P_{\mathrm{S}}\sigma_1^2\lambda_2\lambda_1\cdot K_1\left(2\sqrt{\frac{y\sigma_1^2}{\lambda_1\lambda_2(\eta^2 a_1 P_{\mathrm{S}} - \eta^2 a_2 P_{\mathrm{S}} y)}}\right)}{2\left(\eta^2 a_1 P_{\mathrm{S}} - \eta^2 a_2 P_{\mathrm{S}} y\right)^2\sqrt{\frac{y\sigma_1^2\lambda_2}{\lambda_1(\eta^2 a_1 P_{\mathrm{S}} - \eta^2 a_2 P_{\mathrm{S}} y)}}}\right]
\end{array}\right] dy
\end{aligned}
\tag{39}
$$

2) Under the assumption of perfect SIC, the outage probability at U_2 is given by:

$$\begin{aligned} &P_{\mathrm{OUT}}^{\mathrm{MRC,U_2}} \\ &= \int_{y=0}^{\gamma_{th}} \left[1-\left(1-F_{\gamma_2}\left(\gamma_{th}-y\right)\right)\left(1-F_{\gamma_{U_2,2}}\left(\gamma_{th}-y\right)\right) f_{\gamma_{U_2}^{BC}}\left(y\right)\right] dy \\ &= \int_{y=0}^{\gamma_{th}} \left[\begin{array}{l} 1-\left(1-F_{\gamma_2}\left(\gamma_{th}-y\right)\right)\left(1-F_{\gamma_{U_2,2}}\left(\gamma_{th}-y\right)\right) \\ \times \frac{1}{\lambda_2}\left(\frac{1}{2\sqrt{\frac{y\sigma_2^2\lambda_2}{\lambda_1\eta^2 a_2 P_{\mathrm{S}}}}} \cdot \frac{\sigma_2^2\lambda_2}{\lambda_1\eta^2 a_2 P_{\mathrm{S}}} K_1\left(2\sqrt{\frac{y\sigma_2^2}{\lambda_1\lambda_2\eta^2 a_2 P_{\mathrm{S}}}}\right)\right) \end{array}\right] dy \end{aligned} \tag{40}$$

3) Under the assumption of imperfect SIC, the outage probability at U_1 is given by:

$$\begin{aligned} &P_{\mathrm{OUT}}^{\mathrm{MRC,imp,U_1}} \\ &= \int_{y=0}^{\gamma_{th}} \left[1-\left(1-F_{\gamma_1}\left(\gamma_{th}-y\right)\right)\left(1-F_{\gamma_{U_1,1}}\left(\gamma_{th}-y\right)\right) f_{\gamma_{U_1}^{BC}}\left(y\right)\right] dy \\ &= \int_{y=0}^{\gamma_{th}} \left[\begin{array}{l} 1-\left(1-F_{\gamma_1}\left(\gamma_{th}-y\right)\right)\left(1-F_{\gamma_{U_1,1}}\left(\gamma_{th}-y\right)\right) \\ \times \frac{1}{\lambda_2}\left[\frac{-\eta^2 a_2 P_S {\sigma_1}^2 \lambda_2\lambda_1 \cdot K_1\left(2\sqrt{\frac{y{\sigma_1}^2}{\lambda_1\lambda_2\left(\eta^2 a_1 P_{\mathrm{S}}-\eta^2 a_2 P_{\mathrm{S}} y\right)}}\right)}{2(\eta^2 a_1 P_{\mathrm{S}}-\eta^2 a_2 P_{\mathrm{S}} y)^2\sqrt{\frac{y{\sigma_1}^2\lambda_2}{\lambda_1(\eta^2 a_1 P_{\mathrm{S}}-\eta^2 a_2 P_{\mathrm{S}} y)}}}\right] \end{array}\right] dy \end{aligned} \tag{41}$$

4) Under the assumption of imperfect SIC, the outage probability at U_2 is given by:

$$\begin{aligned} &P_{\mathrm{OUT}}^{\mathrm{MRC,imp,U_2}} \\ &= \int_{y=0}^{\gamma_{th}} \left[1-\left(1-F_{\gamma_2^{imp}}\left(\gamma_{th}-y\right)\right)\left(1-F_{\gamma_{U_2,2}^{imp}}\left(\gamma_{th}-y\right)\right) f_{\gamma_{U_2}^{imp,BC}}\left(y\right)\right] dy \\ &= \int_{y=0}^{\gamma_{th}} \left[\begin{array}{l} 1-\left(1-F_{\gamma_2}\left(\gamma_{th}-y\right)\right)\left(1-F_{\gamma_{U_2,2}}\left(\gamma_{th}-y\right)\right) \\ \times \frac{1}{\lambda_2}\left[\frac{-\eta^2 \Upsilon a_2 P_S {\sigma_1}^2 \lambda_2\lambda_1 \cdot K_1\left(2\sqrt{\frac{y{\sigma_1}^2}{\lambda_1\lambda_2\left(\eta^2 a_1 P_{\mathrm{S}}-\Upsilon\eta^2 a_2 P_{\mathrm{S}} y\right)}}\right)}{2(\eta^2 a_1 P_{\mathrm{S}}-\Upsilon\eta^2 a_2 P_{\mathrm{S}} y)^2\sqrt{\frac{y{\sigma_2}^2\lambda_2}{\lambda_1(\eta^2 a_2 P_{\mathrm{S}}-\Upsilon\eta^2 a_1 P_{\mathrm{S}} y)}}}\right] \end{array}\right] dy \end{aligned} \tag{42}$$

3.3 Ergodic Capacity

Ergodic capacity refers to the average achievable transmission rate over a fading channel, assuming long-term channel variations and ideal coding. This metric indicates the average performance of a system and serves as a benchmark for evaluating communication efficiency over fading channels. The ergodic rate $C_{U_i}^{UAV}$ for the i^{th} user over the UAV link is defined as:

$$C_{U_i}^{UAV} = \frac{1}{2}\int_0^{\infty} \log_2\left(1+m\right) f_M(m) dm \tag{43}$$

$$F_M\left(m\right) = P\left(M \le m\right) = P\left(\min\left(\gamma_i, \gamma_{U_i,i}\right) \le m\right) \tag{44}$$

Under the assumption of perfect SIC, the ergodic capacities associated with UAV transmission for users U_1 and U_2 can be formulated as:

$$C_{U_1}^{UAV} = \frac{1}{2\ln 2}\int_0^{\infty}\frac{1}{1+m}\left[1-\gamma\left(m_1,\frac{m_1}{\bar{\Omega}_1}\left(\frac{m}{B_1-B_2m}\right)^2\right)\right] \cdot\left[1-\left(\frac{m_1}{m_2}\right)^{\frac{m_1-m_2}{2}}\frac{\left(\frac{m}{B_4-B_5m}\right)^{m_1+m_2}}{\Gamma(m_2)\Gamma(m_1+1)} \times G_{1,3}^{3,1}\left(-\frac{m_1m_2}{\Omega_1\Omega_2}\left(\frac{m}{B_4-B_5m}\right)^2\middle|\begin{matrix}1-\frac{m_1+m_2}{2}\\ 1-m_2,\quad -m_1,\quad 0\end{matrix}\right)\right]dm \tag{45}$$

$$C_{U_2}^{UAV} = \frac{1}{2\ln 2}\int_0^{\infty}\frac{1}{1+m}\left[1-\gamma\left(m_2,\frac{m_2}{\bar{\Omega}_2}\left(\frac{m}{B_2}\right)^2\right)\right] \cdot\left[1-\left(\frac{m_1}{m_2}\right)^{\frac{m_1-m_2}{2}}\frac{\left(\frac{m}{B_6}\right)^{m_1+m_2}}{\Gamma(m_2)\Gamma(m_1+1)} \times G_{1,3}^{3,1}\left(-\frac{m_1m_2}{\Omega_1\Omega_2}\left(\frac{m}{B_6}\right)^2\middle|\begin{matrix}1-\frac{m_1+m_2}{2}\\ 1-m_2,\quad -m_1,\quad 0\end{matrix}\right)\right]dm \tag{46}$$

For imperfect SIC, the $C_{U_2}^{UAV}$ is:

$$C_{imp,U_2}^{UAV} = \frac{1}{2\ln 2}\int_0^{\infty}\frac{1}{1+m}\left[1-\gamma\left(m_2,\frac{m_2}{\bar{\Omega}_2}\left(\frac{m}{B_2-B_3m}\right)^2\right)\right] \cdot\left[1-\left(\frac{m_1}{m_2}\right)^{\frac{m_1-m_2}{2}}\frac{\left(\frac{m}{B_6-B_7m}\right)^{m_1+m_2}}{\Gamma(m_2)\Gamma(m_1+1)} \times G_{1,3}^{3,1}\left(-\frac{m_1m_2}{\Omega_1\Omega_2}\left(\frac{m}{B_6-B_7m}\right)^2\middle|\begin{matrix}1-\frac{m_1+m_2}{2}\\ 1-m_2,\quad -m_1,\quad 0\end{matrix}\right)\right]dm \tag{47}$$

In contrast to UAV, with AmBC, there is no need for time slot division as the AmBC device operates by reflecting ambient signals. Therefore, the ergodic capacity $C_{U_i}^{AmBC}$ of the link using AmBC can be expressed as:

$$C_{U_i}^{AmBC} = \frac{1}{2\ln 2}\int_0^{\infty}\ln(1+\gamma)\,f_{\gamma}(\gamma)d\gamma \tag{48}$$

where γ represents the end-to-end SINR from the BS to the ground users U_i through the AmBC link. The ergodic capacities of U_1 and U_2 through AmBC can be formulated

as:

$$C_{U_1}^{AmBC} = \frac{1}{2\ln 2}\int_0^{\infty} \ln(1+\gamma)\frac{1}{\lambda_2} \times \left[\frac{-\eta^2 a_2 P_{\mathrm{S}}\sigma_1^2\lambda_2\lambda_1 \cdot K_1\left(2\sqrt{\frac{\gamma\sigma_1^2}{\lambda_1\lambda_2(\eta^2 a_1 P_{\mathrm{S}}-\eta^2 a_2 P_{\mathrm{S}}\gamma)}}\right)}{2\left(\eta^2 a_1 P_{\mathrm{S}}-\eta^2 a_2 P_{\mathrm{S}}\gamma\right)^2\sqrt{\frac{\gamma\sigma_1^2\lambda_2}{\lambda_1(\eta^2 a_1 P_{\mathrm{S}}-\eta^2 a_2 P_{\mathrm{S}}\gamma)}}}\right] d\gamma \tag{49}$$

$$C_{U_2}^{AmBC} = \frac{1}{2\ln 2}\int_0^{\infty} \ln(1+\gamma)\frac{1}{\lambda_2} \times \left[\frac{1}{2\sqrt{\frac{\gamma\sigma_2^2\lambda_2}{\lambda_1\eta^2 a_2 P_{\mathrm{S}}}}}\cdot\frac{\sigma_2^2\lambda_2}{\lambda_1\eta^2 a_2 P_{\mathrm{S}}}\cdot K_1\left(2\sqrt{\frac{\gamma\sigma_2^2}{\lambda_1\lambda_2\eta^2 a_2 P_{\mathrm{S}}}}\right)\right] d\gamma \tag{50}$$

For imperfect SIC, the $C_{U_2}^{imp,AmBC}$ is:

$$C_{U_2}^{imp,AmBC} = \frac{1}{2\ln 2}\int_0^{\infty} \ln(1+\gamma)\frac{1}{\lambda_2} \times \left[\frac{-\eta^2\Upsilon a_2 P_{\mathrm{S}}\sigma_1^2\lambda_2\lambda_1}{2\left(\eta^2 a_1 P_{\mathrm{S}}-\Upsilon\eta^2 a_2 P_{\mathrm{S}}\gamma\right)^2\sqrt{\frac{\gamma\sigma_2^2\lambda_2}{\lambda_1(\eta^2 a_2 P_{\mathrm{S}}-\Upsilon\eta^2 a_1 P_{\mathrm{S}}\gamma)}}} \cdot K_1\left(2\sqrt{\frac{\gamma\sigma_1^2}{\lambda_1\lambda_2\left(\eta^2 a_1 P_{\mathrm{S}}-\Upsilon\eta^2 a_2 P_{\mathrm{S}}\gamma\right)}}\right)\right] d\gamma \tag{51}$$

The achievable ergodic capacities C_1 and C_2 for the end-to-end link at U_1 and U_2, utilizing signals from both UAV and AmBC with SC applied, are given as [31]:

$$C_1 = \max\left(C_{U_1}^{UAV}, C_{U_1}^{AmBC}\right) \tag{52}$$

$$C_2 = \max\left(C_{U_2}^{UAV}, C_{U_2}^{AmBC}\right) \tag{53}$$

The ergodic capacities for imperfect SIC with $\Upsilon > 0$ for U_1 and U_2 can be derived using a similar method, as detailed in equations (52) and (53).

3.4 System Outage Probability

The system experiences an outage when either of the two users faces an outage. The system outage probability P_{OUT}^{sys} is expressed as follows:

In the case of SC, the P_{OUT}^{sys} is

$$P_{OUT}^{sys} = P_{\mathrm{OUT}}^{\mathrm{SC,U_1}} + P_{\mathrm{OUT}}^{\mathrm{SC,U_2}} - P_{\mathrm{OUT}}^{\mathrm{SC,U_1}} P_{\mathrm{OUT}}^{\mathrm{SC,U_2}} \tag{54}$$

$$P_{OUT}^{sys} = P_{\mathrm{OUT}}^{\mathrm{SC,imp,U_1}} + P_{\mathrm{OUT}}^{\mathrm{SC,imp,U_2}} - P_{\mathrm{OUT}}^{\mathrm{SC,imp,U_1}} P_{\mathrm{OUT}}^{\mathrm{SC,imp,U_2}} \tag{55}$$

For the MRC strategy, the calculation method is the same.

4 RESULTS AND DISCUSSIONS

In this section, we evaluate the proposed network by analyzing its outage probability and ergodic capacity under Nakagami-m fading. Both SC and MRC techniques are considered. Analytical results are verified via MATLAB simulations for various scenarios with a 150 millisecond time slot and an aerial node altitude of 50 meters. All parameter values are listed in Table 1.

Table 1 System parameters for simulation

Parameter	Value	Parameter	Value
α	0.8	β	0.7
ς	0.1	η	0.3
m_1	4	m_2	2
d_{SR}	15m	d_{RU_1}	10m
d_{RU_2}	20m	$a_1 = a_{U,1}$	0.6
$a_2 = a_{U,2}$	0.4	$\overline{\Omega}_1 = \overline{\Omega}_2$	1

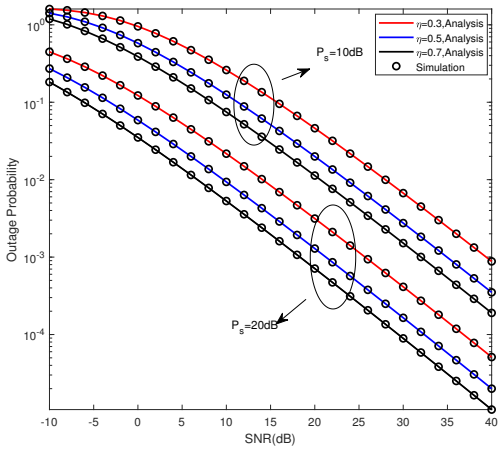


Fig. 2 Variation of outage probability of U_1 with respect γ to the under different η

When the γ ranges from -10 dBm to 40 dBm, the outage probability of U_1 significantly decreases. The Fig. 2 shows that as η increases, the outage probability decreases accordingly. This is because an increase in the backscatter coefficient leads to stronger received signals, which improves signal quality. As a result, the system can decode the transmitted information more effectively and reduce the impact of interference, thus lowering the probability of an outage. Additionally, increasing the backscatter coefficient helps improve the multipath propagation effect, allowing stronger signals to be received through multiple paths and enhancing the system's robustness.

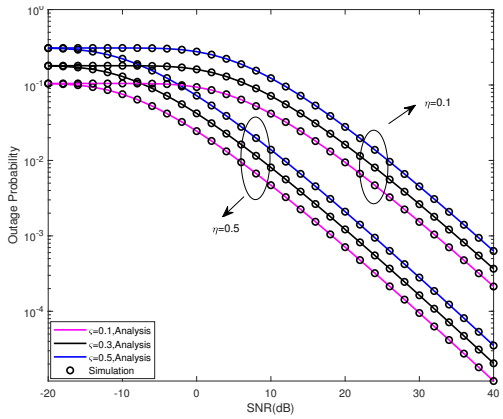


Fig. 3 Variation of outage probability of U_2 with respect to the γ under different ς

This Fig. 3 plots illustrates the variation of the outage probability of the U_2 with respect to the SNR under different path loss conditions. The curves demonstrate that as the SNR increases, the outage probability decreases, indicating that an improvement in signal quality helps to reduce the likelihood of communication outage. Furthermore, the curves under different path loss conditions exhibit noticeable differences, with higher path loss leading to greater signal attenuation and a higher outage probability. This highlights that, even with an increase in SNR, the impact of signal attenuation in poorer propagation environments results in a higher probability of outage.

Fig. 4 shows the variation of the P_{OUT} with respect to the SNR for U_2 under two scenarios of perfect SIC and imperfect SIC with different reflection coefficients. As can be seen from the figure, the outage probability decreases as the SNR increases. The outage probability of decreases as the backscatter coefficient increases. For the same reflection coefficient and SNR, the outage probability is higher under the imperfect SIC scenario compared to the perfect SIC scenario. Furthermore, as the residual interference coefficient increases, the variation in outage probability becomes more significant. This is because the interference encountered during signal processing becomes more severe, leading to a notable increase in the outage probability. The performance degradation caused by imperfect SIC can be compensated by adjusting the backscatter coefficient.

Fig. 5 shows the relationship between the outage probability of U_2 and the threshold γ_{th} . The results consider two different combining techniques, SC and MRC. As γ_{th} increases, the outage probability of U_2 also increases. This indicates that a higher SNR is required to maintain reliable communication with a lower outage probability. MRC outperforms SC in terms of outage probability as it maximizes the SNR by coherently combining multiple received signals, improving signal quality and reducing the outage probability. In contrast, SC only selects the best signal, failing to fully utilize the potential of all available signals.

Fig. 6 compares the performance of the proposed scheme with and without AmBC technology. The system outage probability is analyzed in terms of its impact on SNR. It can be observed that as the SNR increases, the system outage probability decreases

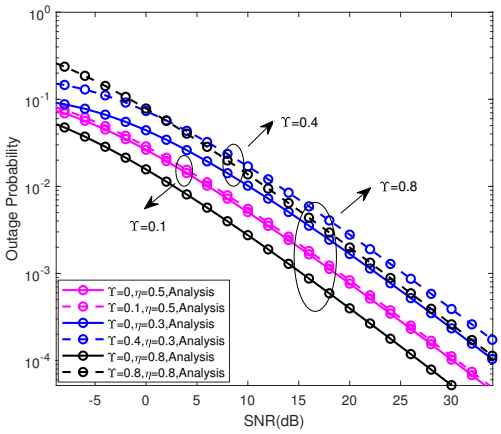


Fig. 4 Variation of outage probability of U_2 under SIC and imperfect SIC

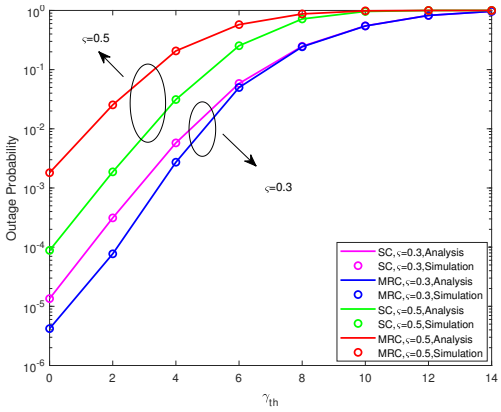


Fig. 5 Variation of outage probability of U_2 under MRC and SC

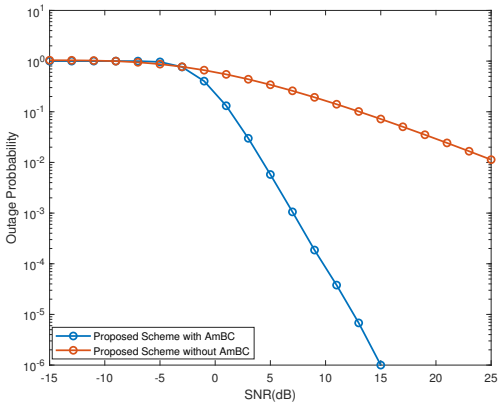


Fig. 6 Performance Comparison of the Proposed Scheme with the Scheme without AmBC

in both cases. However, the outage probability is lower when AmBC technology is employed. This is because AmBC enables low-power data transmission by reflecting existing ambient RF signals, thereby enhancing the signal quality. By increasing the backscatter coefficient, AmBC improves the multipath propagation effect, resulting in stronger received signals, which in turn increases communication reliability and reduces interference, leading to a lower outage probability.

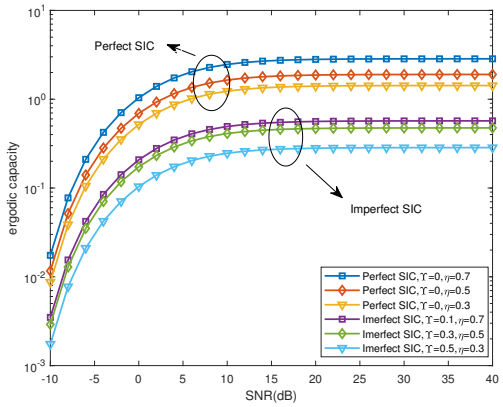


Fig. 7 The Ergodic Capacity of U_2 under Perfect SIC and Imperfect SIC with Respect to SNR

In Fig. 7, the ergodic capacity curves as a function of SNR are plotted for both perfect SIC and imperfect SIC cases, revealing some important observations regarding the impact of SNR and the use of perfect SIC on system performance. Firstly, the ergodic capacity increases with the SNR due to the improved signal quality at higher SNR, which enhances the system's transmission capability. And as can be seen from the figure, the ergodic capacity of U_2 is higher under perfect SIC compared to imperfect SIC. This is because perfect SIC allows for more effective interference cancellation, resulting in better signal quality and higher capacity.

5 CONCLUSION

This paper investigates a UAV-AmBC integrated scheme based on NOMA networks. To accurately model wireless channel conditions, both Nakagami-m and Rayleigh fading are considered in the uplink and downlink scenarios through the UAV and AmBC channels. Specifically, Nakagami-m fading is assumed for the channels from the BS to the UAV and from the UAV to the ground users, while Rayleigh fading is considered for the channels from the BS to the BC and from the BC to the ground users. Additionally, diversity combining techniques, such as SC and MRC, are applied to the signals from both the UAV and AmBC for the ground users, with MRC observed to outperform SC. The analysis primarily focuses on evaluating the outage and ergodic capacity performance of the network through the development of analytical expressions. AmBC plays a crucial role in enhancing the signal by reflecting existing ambient RF signals, with the backscatter coefficient directly affecting its ability to improve signal quality.

Compared to perfect SIC, imperfect SIC leads to performance degradation. However, a proper allocation of the backscatter coefficient and an appropriate SNR threshold can improve both the outage and ergodic capacity. These findings highlight the potential of the UAV-AmBC system in improving network performance under realistic channel conditions.

Appendix A Section title of first appendix

A.1 Proof of (27)

Assuming $v = |h_{\mathrm{SR}}|^2 |h_{\mathrm{RU}_i}|^2$, are given as follows [8][9],

$$f_{|v|^2}(v) = \frac{4v^{m_1+m_2-1} {m_1}^{m_1} {m_2}^{m_2}}{\Gamma(m_1)\Gamma(m_2)(\Omega_1\Omega_2)^{\frac{m_1+m_2}{2}}} K_{m_1-m_2}\left(2v\sqrt{\frac{m_1 m_2}{\Omega_1\Omega_2}}\right) \tag{A1}$$

Respectively, where $K_n(\cdot)$ is the modified Bessel function of the second kind.

Make $\mu = m_1 + m_2$,$\nu = m_1 - m_2$,$a = 2\sqrt{\frac{m_1 m_2}{\Omega_1\Omega_2}}$,$z = \frac{\gamma_{th}}{B_4 - B_5\gamma_{th}}$, According to [9], get the equation:

$$\int_0^z x^{\mu-1} K_\nu(ax)dx = \frac{2^{\mu-2} z^\mu \Gamma\left(\frac{\mu-\nu}{2}\right)\Gamma\left(\frac{\mu+\nu}{2}\right)}{a^\mu} {}_1F_2\left(\frac{\mu}{2}; \frac{\mu-\nu}{2}, \frac{\mu+\nu}{2}+1; \frac{a^2 z^2}{4}\right) \tag{A2}$$

where $\frac{\mu-\nu}{2} = m_2$,$\frac{\mu+\nu}{2} = m_1$,$a^2 = 4\frac{m_1 m_2}{\Omega_1\Omega_2}$,$a^2 z^2 = \frac{m_1 m_2}{\Omega_1\Omega_2} z^2$.

Furthermore,$\left(2\sqrt{\frac{m_1 m_2}{\Omega_1\Omega_2}}\right)^{m_1+m_2} = 2^{m_1+m_2}\left(\frac{m_1 m_2}{\Omega_1\Omega_2}\right)^{\frac{m_1+m_2}{2}}$, $2^{m_1+m_2-2}/2^{m_1+m_2} = \frac{1}{4}$.

After the calculation, Eq. (57) can be written as:

$$\begin{aligned}
&F_{\gamma_{U_1,1}}(\gamma_{th}) \\
&= P\left(\int_0^{\frac{\gamma_{th}}{B_4 - B_5\gamma_{th}}} \frac{4x^{m_1+m_2-1} {m_1}^{m_1} {m_2}^{m_2}}{\Gamma(m_1)\Gamma(m_2)(\Omega_1\Omega_2)^{\frac{m_1+m_2}{2}}} K_{m_1-m_2}\left(2x\sqrt{\frac{m_1 m_2}{\Omega_1\Omega_2}}\right) dx\right) \\
&= \left(\frac{m_1}{m_2}\right)^{\frac{m_1-m_2}{2}} \left(\frac{\gamma_{th}}{B_4 - B_5\gamma_{th}}\right)^{m_1+m_2} {}_1F_2\left(\frac{m_1+m_2}{2}; m_2, m_1+1; \frac{m_1 m_2}{\Omega_1\Omega_2}\left(\frac{\gamma_{th}}{B_4 - B_5\gamma_{th}}\right)^2\right)
\end{aligned} \tag{A3}$$

According to [26]

$${}_1F_2(a; b, c; x) = \frac{1}{\Gamma(b)\Gamma(c)} G_{1,3}^{3,1}\left(-x \,\middle|\, \begin{matrix} 1-a \\ 1-b, \quad 1-c, \quad 0 \end{matrix}\right) \tag{A4}$$

where ${}_1F_2(a; b, c; x)$ is a generalized hypergeometric function that represents a series expansion with specific parameters, while the $G_{1,3}^{3,1}\left(-x \,\middle|\, \begin{matrix} 1-a \\ 1-b, \quad 1-c, \quad 0 \end{matrix}\right)$ is a Meijer G-function, a more generalized class of special functions used to represent complex integrals and series with multiple parameters.

Finally, Eq. (59) simplifies to:

$$
\begin{aligned}
F_{\gamma_{U_1,1}}(\gamma_{th}) = & \left(\frac{m_1}{m_2}\right)^{\frac{m_1-m_2}{2}} \frac{\left(\frac{\gamma_{th}}{B_4-B_5\gamma_{th}}\right)^{m_1+m_2}}{\Gamma(m_2)\Gamma(m_1+1)} \\
& \cdot G_{1,3}^{3,1}\left(-\frac{m_1 m_2}{\Omega_1\Omega_2}\left(\frac{\gamma_{th}}{B_4-B_5\gamma_{th}}\right)^2 \middle| \begin{matrix} 1-\frac{m_1+m_2}{2} \\ 1-m_2, \quad -m_1, \quad 0 \end{matrix}\right)
\end{aligned}
\tag{A5}
$$

the proof is completed.

A.2 Proof of (31)

The calculation process of Eq. (31) is as follows:

$$
\begin{aligned}
F_{\gamma_{\mathrm{U}_1}^{\mathrm{BC}}}(\gamma_{th}) &= P\left(\gamma_{\mathrm{U}_1}^{\mathrm{BC}} \le \gamma_{th}\right) \\
&= P\left(\frac{\eta^2 a_1 P_{\mathrm{S}} |h_{\mathrm{SB}}|^2 |h_{\mathrm{BU}_1}|^2}{\eta^2 a_2 P_{\mathrm{S}} |h_{\mathrm{SB}}|^2 |h_{\mathrm{BU}_1}|^2 + \sigma_1^2} \le \gamma_{th}\right) \\
&= P\left[|h_{\mathrm{SB}}|^2 |h_{\mathrm{BU}_1}|^2 \le \frac{\gamma_{th}\sigma_1^2}{\eta^2 a_1 P_{\mathrm{S}} - \eta^2 a_2 P_{\mathrm{S}}\gamma_{th}}\right] \\
&= \int_0^{\infty}\int_0^{\frac{\gamma_{th}\sigma_1^2}{(\eta^2 a_1 P_{\mathrm{S}} - \eta^2 a_2 P_{\mathrm{S}}\gamma_{th})y}} f_X(x)\, f_Y(y)\, dxdy \\
&= \int_0^{\infty}\int_0^{\frac{\gamma_{th}\sigma_1^2}{(\eta^2 a_1 P_{\mathrm{S}} - \eta^2 a_2 P_{\mathrm{S}}\gamma_{th})y}} \frac{1}{\lambda_1}\exp\left(-\frac{x}{\lambda_1}\right) dx \frac{1}{\lambda_2}\exp\left(-\frac{y}{\lambda_2}\right) dy \\
&= \frac{1}{\lambda_2}\int_0^{\infty}\exp\left(-\frac{y}{\lambda_2}\right)\left[1-\exp\left(-\frac{\gamma_{th}\sigma_1^2}{\lambda_1\left(\eta^2 a_1 P_{\mathrm{S}} - \eta^2 a_2 P_{\mathrm{S}}\gamma_{th}\right)y}\right)\right] dy \\
&= \frac{1}{\lambda_2}\left[\int_0^{\infty}\exp\left(-\frac{y}{\lambda_2}\right) dy - \int_0^{\infty}\exp\left[-\left(\frac{y}{\lambda_2} + \frac{\gamma_{th}\sigma_1^2}{\lambda_1\left(\eta^2 a_1 P_{\mathrm{S}} - \eta^2 a_2 P_{\mathrm{S}}\gamma_{th}\right)y}\right)\right] dy\right] \\
&= \frac{1}{\lambda_2}\left[\lambda_2 - 2\left(A\cdot\frac{1}{\lambda_2}\right)^{\frac{1}{2}} K_1\left(2\sqrt{A}\,\lambda_2\right)\right] \\
&= 1 - \frac{1}{\lambda_2}\sqrt{\frac{\gamma_{th}\sigma_1^2\lambda_2}{\lambda_1\left(\eta^2 a_1 P_{\mathrm{S}} - \eta^2 a_2 P_{\mathrm{S}}\gamma_{th}\right)}} K_1\left(2\sqrt{\frac{\gamma_{th}\sigma_1^2}{\lambda_1\lambda_2\left(\eta^2 a_1 P_{\mathrm{S}} - \eta^2 a_2 P_{\mathrm{S}}\gamma_{th}\right)}}\right)
\end{aligned}
\tag{A6}
$$

where $\frac{\gamma_{th}{\sigma_1}^2}{\lambda_1(\eta^2 a_1 P_{\mathrm{S}} - \eta^2 a_2 P_{\mathrm{S}}\gamma_{th})y} = \frac{A}{y}$. According to [11],

$$
\int_0^{\infty}\exp\left[-\left(\frac{y}{\lambda_2}+\frac{A}{y}\right)\right] dy = 2\left(A\cdot\frac{1}{\lambda_2}\right)^{1/2} K_1\left(2\sqrt{A}\lambda_2\right) \tag{A7}
$$

where $K_1(\cdot)$ is the first-order value of the modified Bessel function of the second kind. The proof is completed.

References

[1] Gustavsson, U., Frenger, P., Fager, C., Eriksson, T., Zirath, H., Dielacher, F., Studer, C., Pärssinen, A., Correia, R., Matos, J.N., Belo, D., Carvalho, N.B.: Implementation challenges and opportunities in beyond-5g and 6g communication. IEEE Journal of Microwaves **1**(1), 86–100 (2021) https://doi.org/10.1109/JMW.2020.3034648

[2] Yao, C., Liu, Y., Wei, X., Wang, G., Gao, F.: Backscatter technologies and the future of internet of things: Challenges and opportunities. Intelligent and Converged Networks **1**(2), 170–180 (2020) https://doi.org/10.23919/ICN.2020.0013

[3] Ye, Y., Shi, L., Chu, X., Lu, G.: On the outage performance of ambient backscatter communications. IEEE Internet of Things Journal **7**(8), 7265–7278 (2020) https://doi.org/10.1109/JIOT.2020.2984449

[4] Peng, H., Liu, M., Yang, L., Zeng, M., Wang, J., Guo, K., Li, X.: Ambient backscatter communication symbiotic intelligent transportation systems: Covertness performance analysis and optimization. IEEE Transactions on Consumer Electronics **70**(1), 1833–1844 (2024) https://doi.org/10.1109/TCE.2023.3329675

[5] Zhao, W., Wang, G., Atapattu, S., Tellambura, C., Guan, H.: Outage analysis of ambient backscatter communication systems. IEEE Communications Letters **22**(8), 1736–1739 (2018) https://doi.org/10.1109/LCOMM.2018.2842774

[6] Yadav, S., Gour, R., Gurjar, D.S., Bhatnagar, M.: Ambient backscatter communications with multi-tag selection: Outage performance analysis. IEEE Communications Letters **28**(12), 2884–2888 (2024) https://doi.org/10.1109/LCOMM.2024.3477726

[7] Ali, M., Sharma, P.K.: Outage analysis of multi-tag ambient backscatter systems under rfhis and outdated csi. IEEE Wireless Communications Letters **14**(4), 1059–1063 (2025) https://doi.org/10.1109/LWC.2025.3531466

[8] Liu, Y., Zhou, Z., Ye, Y., Li, X., Geng, M., Nallanathan, A.: Outage performance analysis for mutualistic symbiotic backscatter communication systems. IEEE Transactions on Vehicular Technology **74**(2), 3457–3462 (2025) https://doi.org/10.1109/TVT.2024.3472042

[9] Qiao, S., Zhao, J., Adeke, J.M., Chen, K., Liu, G.: On the covert performance of ambient backscatter communications. In: 2023 International Conference on Networks, Communications and Intelligent Computing (NCIC), pp. 128–140 (2023). https://doi.org/10.1109/NCIC61838.2023.00028

[10] Ye, Y., Tian, Y., Chu, X., Sun, S., Lu, G.: Outage performance of relay-assisted mutualistic backscatter communications under energy-causality constraint. IEEE

Transactions on Communications **73**(7), 4616–4629 (2025) https://doi.org/10.1109/TCOMM.2024.3511712

[11] Solanki, S., Gautam, S., Sharma, S.K., Chatzinotas, S.: Ambient backscatter assisted co-existence in aerial-irs wireless networks. IEEE Open Journal of the Communications Society **3**, 608–621 (2022) https://doi.org/10.1109/OJCOMS.2022.3163574

[12] Ahmed, M., Shahwar, M., Khan, F., Ullah Khan, W., Ihsan, A., Sadiq Khan, U., Xu, F., Chatzinotas, S.: Noma-based backscatter communications: Fundamentals, applications, and advancements. IEEE Internet of Things Journal **11**(11), 19303–19327 (2024) https://doi.org/10.1109/JIOT.2024.3391219

[13] Hesam, A., Bastami, A.H., Abdel-Hafez, M.A.: Performance analysis of noma-based transmission in two-way relay network. IEEE Access **12**, 37051–37068 (2024) https://doi.org/10.1109/ACCESS.2024.3374636

[14] Nguyen, T.H., Phung, K.H.: Ambc-assisted mobility vehicle system with partial noma transmission. IEEE Open Journal of the Communications Society **5**, 6686–6696 (2024) https://doi.org/10.1109/OJCOMS.2024.3474772

[15] Bisen, S., Jose, J., Ding, Z., Choi, K., Bhatia, V.: On performance of backscatter-noma systems: Symbiotic communication for iot devices. IEEE Transactions on Vehicular Technology **73**(10), 15854–15859 (2024) https://doi.org/10.1109/TVT.2024.3415353

[16] Hoa Nguyen, T., Phung, K.H.: Investigation of backscatter-enabled partial noma systems: Outage probability and ergodic capacity evaluation. IEEE Access **12**, 64114–64125 (2024) https://doi.org/10.1109/ACCESS.2024.3396824

[17] Hai, N.T., Khoa, D.L.: Backcom-aided noma systems: A simultaneous process of covertness and information at tag. IEEE Wireless Communications Letters **14**(1), 83–87 (2025) https://doi.org/10.1109/LWC.2024.3487952

[18] Pei, X., Wang, X., Huang, M., Chen, Y., Li, X., Tsiftsis, T.A.: Physical-layer security in ambc-noma networks with random eavesdroppers. IEEE Internet of Things Journal **12**(12), 18628–18642 (2025) https://doi.org/10.1109/JIOT.2025.3557167

[19] Mozaffari, M., Saad, W., Bennis, M., Nam, Y.-H., Debbah, M.: A tutorial on uavs for wireless networks: Applications, challenges, and open problems. IEEE Communications Surveys and Tutorials **21**(3), 2334–2360 (2019) https://doi.org/10.1109/COMST.2019.2902862

[20] Huang, H., Wei, Y., Liang, L., Yin, Z., Zhang, N.: On the analysis of multisource cooperative network assisted by uav relays with co-channel interference. IEEE Journal on Miniaturization for Air and Space Systems **6**(2), 144–156 (2025) https:

//doi.org/10.1109/JMASS.2024.3519344

[21] Xia, Y., Liu, W., Zhang, K., Xu, C., Huang, D.: Bounding the path loss in uav-assisted wireless sensor networks. IEEE Antennas and Wireless Propagation Letters **23**(8), 2341–2345 (2024) https://doi.org/10.1109/LAWP.2024.3389782

[22] Pandey, G.K., Gurjar, D.S., Yadav, S., Jiang, Y., Yuen, C.: Uav-assisted communications with rf energy harvesting: A comprehensive survey. IEEE Communications Surveys and Tutorials **27**(2), 782–838 (2025) https://doi.org/10.1109/COMST.2024.3425597

[23] Wu, X., Jiang, X., Li, B., Zhao, N., Li, P., Li, Y., Nallanathan, A.: Rate maximization of uav-assisted ambient backscatter communications. IEEE Wireless Communications Letters **13**(3), 706–710 (2024) https://doi.org/10.1109/LWC.2023.3340242

[24] Yang, H., Ye, Y., Chu, X., Sun, S.: Energy efficiency maximization for uav-enabled hybrid backscatter-harvest-then-transmit communications. IEEE Transactions on Wireless Communications **21**(5), 2876–2891 (2022) https://doi.org/10.1109/TWC.2021.3116509

[25] Ning, B., Yi, M., Xu, Y., Li, J., Hao, W.: Aav-assisted ambc network: Performance analysis in nakagami-m fading channel. IEEE Transactions on Vehicular Technology **74**(5), 6966–6978 (2025) https://doi.org/10.1109/TVT.2025.3528011

[26] Jiang, X., Sheng, M., Zhao, N., Liu, J., Niyato, D., Yu, F.R.: Outage analysis of uav-aided networks with underlaid ambient backscatter communications. IEEE Transactions on Wireless Communications **22**(11), 7492–7505 (2023) https://doi.org/10.1109/TWC.2023.3251979

[27] Jia, S., Wang, R., Lou, Y., Wang, N., Zhang, D., Singh, K., Mumtaz, S.: Secrecy performance analysis of uav-assisted ambient backscatter communications with jamming. IEEE Transactions on Wireless Communications **23**(12), 18111–18125 (2024) https://doi.org/10.1109/TWC.2024.3461800

[28] Han, R., Bai, L., Wen, Y., Liu, J., Choi, J., Zhang, W.: Uav-aided backscatter communications: Performance analysis and trajectory optimization. IEEE Journal on Selected Areas in Communications **39**(10), 3129–3143 (2021) https://doi.org/10.1109/JSAC.2021.3088676

[29] Gan, X., Jiang, Y., Wang, Y., Hong, D., Wang, Z.: Sum rate maximization for uav assisted noma backscatter communication system. In: 2023 6th World Conference on Computing and Communication Technologies (WCCCT), pp. 19–23 (2023). https://doi.org/10.1109/WCCCT56755.2023.10052259

[30] Du, Y., Chen, Z., Hao, J., Guo, Y.: Joint optimization of trajectory and communication in multi-uav assisted backscatter communication networks. IEEE Access

10, 40861–40871 (2022) https://doi.org/10.1109/ACCESS.2022.3165159

[31] Kim, J.-H., Lee, M.-C., Lee, T.-S.: Generalized uav deployment for uav-assisted cellular networks. IEEE Transactions on Wireless Communications **23**(7), 7894–7910 (2024) https://doi.org/10.1109/TWC.2023.3345839